NEAR FIELD ANALYSIS OF A WIDEBAND LOG-SPIRAL ANTENNA FOR 1-2 GHZ GPR

Mike Phelan Hong Su Joe LoVetri
Department of Electrical and Computer Engineering
University of Manitoba, 15 Gillson Street, Winnipeg, Manitoba, R3T 5V6
mphelan@ee.umaintoba.ca shong@ee.umaintoba.ca lovetri@ee.umanitoba.ca

Abstract

The log-spiral antenna described in this paper is part of the ultra-wideband stepped frequency Ground Penetrating Radar (GPR) for subsurface landmine detection currently being developed at the University of Manitoba. Log-spiral antennas possess many features that are desirable in such a radar system: low profile, high bandwidth, and circular polarization. Firstly, the design and construction of the antenna are described. The antenna is fitted with a wideband balun to balance the current between the two arms of the spiral. An absorber loaded cavity is used behind the antenna to help direct the energy into the ground and keep it from radiating into the air. Next, a study of the far and near fields of the antenna, via simulations and measurements, is presented. The near fields are measured using short coaxial E-field probes at electrically short distances from the antenna and agree well with simulations.

Key Words: *log-spiral antenna; Ground Penetrating Radar.*

1. Introduction

The planar log-spiral antenna is a broadband, circularly polarized and low profile antenna which shows much promise for wideband stepped frequency GPR for humanitarian demining applications [1]. When GPR is used to detect targets which are in close proximity to its ground coupled antenna, as is the case for the detection of land mines, the target will be in the antenna's near field. Therefore, it is the near field which plays the important role in the detection of mines and mine like targets [2]. However, little information is available regarding the near field characteristics of wideband GPR antennas.

In this paper we will discuss the requirements of GPR antennas and the prospects of the loaded cavity-backed log-spiral antenna as an appropriate option for the 1-2 GHz stepped frequency continuous wave (SFCW) GPR antenna currently being developed at the University of Manitoba (UofM). Near field characteristics will be presented and the results of near field simulations using a method of moments commercial software package will be shown.

The GPR system needs to achieve adequate range resolution (i.e., depth resolution) and needs to operate at sufficiently low frequencies to limit attenuation in a lossy ground. The depth resolution ΔR is dictated by the system bandwidth according to the equation $\Delta R = v/2B$ but the choice of bandwidth, B, is limited by the depth of penetration in the ground medium. If the upper frequency is selected too high, the GPR system risks not being able to "see" the target at all due to the high ground losses at high frequencies [3]. Cooke and Gladwin [4] have reported that for typical Australian soil samples at 10% moisture content, the loss tangent could be expected to decrease from over 0.6 at 100 MHz to less than 0.15 at 1.5 GHz. For soil samples with 0% moisture content, the loss tangent could be expected to range from 0.2 at 100 MHz to slightly less than 0.1 at 1.5 GHz. The GPR system being developed at the UofM is designed to operate over a 1-2 GHz bandwidth. High directivity is an advantage, however high directivity is not a common feature in wideband antennas. The polarization of the antenna radiation can be an extremely important factor in GPR. Circular polarization is often preferred because it makes it easier to reject ground reflections and to discriminate between a landmine and ground [1]. For signal processing reasons it is desirable to avoid any nulls in the antenna field pattern [5].

2. Mechanical and Physical Considerations

Mechanical robustness, small size, and light weight are crucial features of a practical GPR antenna solution. Various element antennas, horn antennas, and frequency independent antennas have been used in the past for GPR. Element antennas such as the shielded dipole, bow-tie, and resistively loaded dipoles are perhaps the most common antennas in GPR applications [3]. These are linearly

Proceedings of the 2002 IEEE Canadian Conference on Electrical & Computer Engineering
0-7803-7514-9/02/$17.00 © 2002 IEEE

polarized, have a limited bandwidth and exhibit poor radiation characteristics for GPR (low directivity and bi-directional patterns). One such antenna is the capacitively loaded bow-tie antenna proposed by Yarovoy *et. al.* [6].

Horn antennas possess many desirable features, however at the frequencies of interest they are large and bulky. A dielectric loaded TEM horn has been proposed for a pulsed radar GPR system in [6]. By loading a horn with a dielectric of dielectric constant ε_r, the electrical length of the antenna will be extended by a factor of $\sqrt{\varepsilon_r}$ and therefore the physical size of the antenna can be reduced or the gain can be increased. A better impedance match can be achieved if the electrical properties of the ground are matched to the loading dielectric [6].

Frequency independent antennas are entirely defined by angle variables and have a shape that is invariant to scale. Since a practical antenna must have finite dimensions, actual frequency independent antennas cannot be entirely defined by angles and are therefore limited in bandwidth by their minimum and maximum dimensions [7]. Bandwidths of up to 10:1 or more are common. Examples of frequency independent antennas are the Archimedean spiral, log-periodic and log-spiral antennas. The planar log-spiral antenna is broadband, circularly polarized and low profile and shows much promise as an antenna for wide band stepped frequency GPR applications [1]. The log-spiral printed strip or slot antenna is a bi-directional antenna with two main lobes positioned on either side of the antenna's geometric plane similar to the Archimedean spiral antenna. For unidirectional radiation an absorbing cavity is traditionally used to absorb the radiation in one hemisphere [8]. The absorbing materials in the cavity aids in reducing the destructive interference in the forward beam to maintain the integrity of the antenna field pattern's wideband characteristics [8]. Thus, at least half of the power radiated from the antenna will be absorbed in the cavity and the antenna will exhibit low efficiency. Several attempts to implement spiral antennas with tightly spaced ground planes have been made. Gschwendtner & Wiesbeck have succeeded in producing a 2:1 bandwidth for a ground plane spacing of $\lambda_{max}/4$. Volakis *et. al* [10] have had success with a tightly spaced ground plane over an Archimedian spiral slot antenna, which has similar characteristics to the log-spiral.

The planar spiral antenna is a balanced, two arm, self complementary design, as described by Babinet's principle [11], which is defined by the logarithmic spiral curve

$$\phi(\rho) = a^{-1}\ln(\rho/\rho_i) \qquad (1)$$

where ρ is the radial distance in the direction of the angle ϕ and ρ_i is the initial radius of the curve. The initial radius a (or the spiral rate constant $1/a$) are given by

$$a = \ln(\rho_f/\rho_i)/\phi_f \qquad (2)$$

where ρ_f and ϕ_f are the final values of the curve radius and angle respectively.

The planar log spiral is defined by four such curves, each describing one of the four metallic edges of the antenna. Each curve is offset by an angle δ from one another. In the case of a self complementary design, $\delta = \pi/2$ and the spacing between antenna arms is the same as the width of the arms. The inter-curve angle δ defines the initial and final angles for each curve as

$$\phi_i = n\delta,\ \phi_f = n\delta + 2\pi N \qquad (3)$$

where n is the particular antenna edge ($n = \{1,2,3,4\}$ for a two arm spiral with 4 edges) and N is the total number of turns in the spiral. The two antenna arms are 180^o apart from one another. For our antenna, $\rho_i = 3$ mm, $\rho_f = 130$ mm, $N = 1.5$ to give a spiral rate of 0.343. The spiral arms are tapered with a circular path of constant radius $r = 130$ mm which apparently minimizes the lower limit of frequency independence for a given log-spiral diameter. The log-spiral structure is mounted on a dielectric laminate (MC5 60 MIL HF) of thickness 0.06 inches having relative permittivity $\varepsilon_r = 3.2$. The arms are covered with a copper sheet and the spaces between the arms are open dielectric laminate to produce the spiral patch antenna. It should be noted that the log-spiral antenna configuration can be successfully implemented in a slot of similar dimensions cut out of a sheet of metal [11].

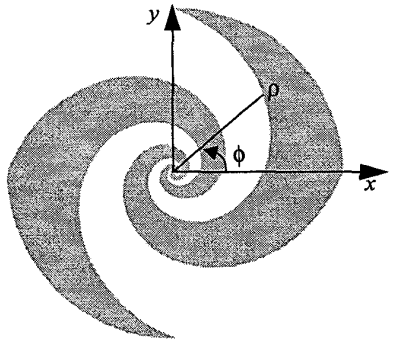

Fig. 1. Geometry of the planar log-spiral antenna.

A wideband M/A-Com ETC1-1-13 ferrite transformer configured as a balun is used to deliver a balanced current to the spiral arms from the unbalanced coaxial feed line. In order to maintain both geometrical and electrical balance, the balun, which is physically very small, is surface mounted directly on the dielectric surface at the spiral origin. The current amplitude balance of the balun was measured to have less than 1 dB of imbalance over the operational frequency.

The spiral/dielectric unit is mounted on a metallic cavity having a diameter of 28 cm. The cavity is loaded with a flat piece SFC-4, 4 in (10 cm) absorber from Cuming Corp.

The absorbing foam is separated from the antenna by 2 in (5 cm) of polystyrene foam as shown in Fig. 2.

The VSWR of the entire antenna unit measured across a bandwidth of 0.5-6 GHz showed that, except for a few exceptions, the VSWR remains below 3 dB across a 12:1 bandwidth and in particular is below 2 dB throughout the operational band of 1-2 GHz.

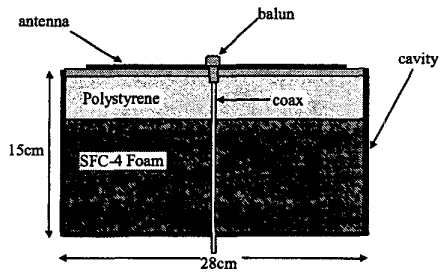

Fig. 2. Geometry of the cavity backed planar spiral antenna cavity.

3. Numerical Simulations

Numerical simulations were carried out using the Ensemble software package by Ansoft© which uses the method of moments. When creating the spiral antenna geometry, 58 points per curve were used to approximate the four curve edges of the log-spiral (two curve edges define one spiral arm). The radius of the outer antenna edge is 130 mm and a simulation area of 300 x 300 mm^2 was used to calculate the near field surface plots. A 2.5D probe/gap source model was used at the center of the two antenna arms. The antenna is fed by two probes extended on two vias with amplitude 1 A and arm phases of 0^o and 180^o respectively. The cavity was approximated by 16 vias protruding upwards from the infinite ground and distributed evenly around the spiral at a radius of 140 mm. These vias measuring 1 mm in radius were spaced at less than $\lambda_{min}/4$, where λ_{min} = 150 mm is the shortest wavelength in the operational bandwidth, corresponding to 2GHz. The simulation geometry is shown in Fig. 3.

To approximately simulate the layer of absorbing foam in the cavity, the electrical characteristics of the foam were approximated by values of real permittivity $\varepsilon_{foam} = 2$, bulk conductivity σ = 0.073 mho/m, and loss tangent tan δ = 0.327. The polystyrene foam separating the dielectric and absorbing foam was approximated as air.

Near field simulations were carried out for three elevation planes (i.e., z = constant planes): z = 5 cm, 10 cm and 20 cm from the antenna, and at three frequencies: 1 GHz, 1.5 GHz and 2 GHz at each elevation plane.

Figures 4 and 5 show the simulated far field patterns at 1.5 GHz for the spiral antenna without and with loaded cavity, respectively. As expected, after the absorber loaded cavity is used, the field pattern becomes unidirectional at a cost of about 10 dB decrease to the lobe peak. Near field solutions, shown below, were obtained for the nine configurations in the form of a 30 cm by 30 cm surface plots at the prescribed distances of 5 cm, 10 cm and 20 cm from the antenna.

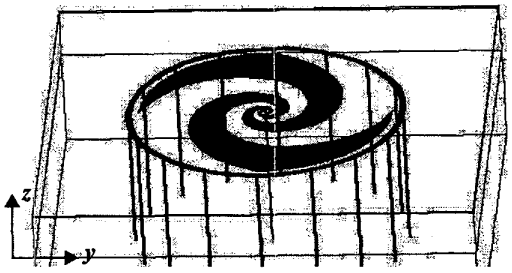

Fig. 3. Ensemble Simulation Geometry.

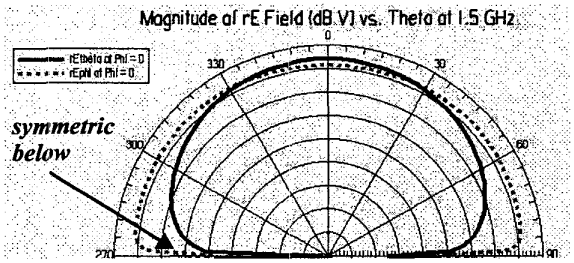

Fig. 4. Far Field Pattern: no foam and no cavity.

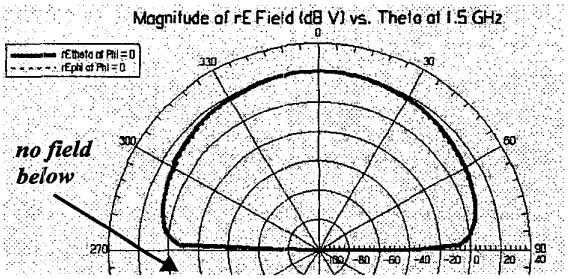

Fig. 5. Far Field Pattern: antenna with foam-loaded cavity

4. Near Field Measurements

To measure the electric field intensity in the near field, electric field probes were fashioned from 50 Ω semi-rigid coax cable with the center conductor protruding 1cm to form an electrically short monopole. Two similar probes were used to take the measurements, one straight probe for E_z measurements and one probe with a 90° bend for E_x and E_y measurements. Although such a probe is not terribly

sensitive, it has the advantage of being electrically small to offer high resolution measurements. The probe VSWR is not very flat over the operational bandwidth but this does not matter as all data at a given frequency are normalized to get rid of probe biases as well as other sources of bias.

An experimental apparatus was constructed to measure the near field electric field components at the 5, 10, and 20 cm elevation planes along both the x and y axes. Measurements were taken at 1 cm intervals across a 30 cm line centered at the antenna's geometric center for a total of 31 measurements per experiment. All measurements were taken in an anechoic housing within a shielded enclosure to reduce noise and resonances in the measurements. These were made at 1 GHz, 1.5 GHz and 2 GHz at each elevation plane. The antenna was carefully moved across the near field probe at increments of 1 cm while the probe was held stationary. All measurements were done using an HP 8546A spectrum analyzer positioned outside of the shielded enclosure. Since only the relative near field intensities of the antenna are of interest here, all data sets were normalized to the E_{total} maximum. Simulations for E_{total}, E_x, E_y and E_z were performed and compared with the experimental results recorded along the x and y axes. Most of the experimental results compare well with axial cuts taken along the corresponding axes of the simulation plots. Figures 6 through 9 show the near field pattern simulations plotted for each electric field component at z = 5 cm at 2GHz. Figures 10 and 11 show the experimental near field data taken along the x and y axes respectively.

Both experimental data and simulated calculations show that the electric field intensity in the near field is markedly different than radiation patterns in the far field where only one intensity maximum is revealed. The near field pattern possesses a more complicated distribution than the far field radiation. When comparing the simulations to the experimental data, we get the expected small peaks and valleys at the estimated distances for all E components while testing along y axis. The x axis experimental data shows that the trends for E_y and E_z are very similar to the simulation result however the expected two valleys for the E_x component and E_{total} are not resolved. The peak of the E_x component appears about 5 cm off the antenna geometric center. All experimental data showed that the E_z components in all cases were smaller than their corresponding E_x and E_y components. Generally the E_z component seems to have a minimum at the origin (0 cm) for all cases. Furthermore it is observed that the data trends along both x and y axes are not entirely symmetric with respect to the center in terms of amplitude and position of maxima and minima. Symmetry discrepancies between the results are most likely due to imperfect phase and amplitude balance provided by the ferrite balun.

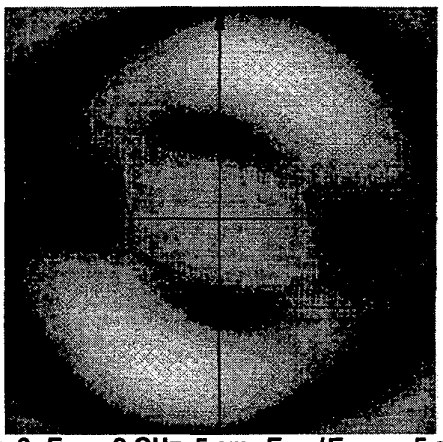

Fig. 6. E_{total}, 2 GHz, 5 cm, $E_{max}/E_{min} \approx$ 5 dB.

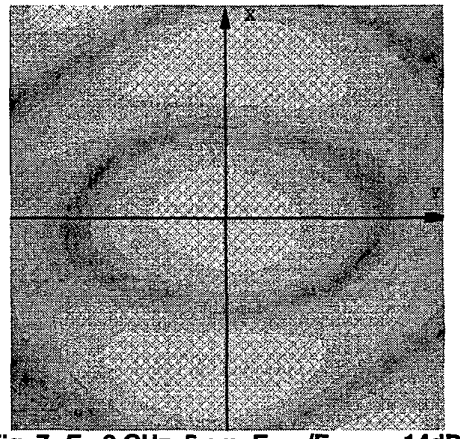

Fig. 7. E_x, 2 GHz, 5 cm, $E_{max}/E_{min} \approx$ 14dB.

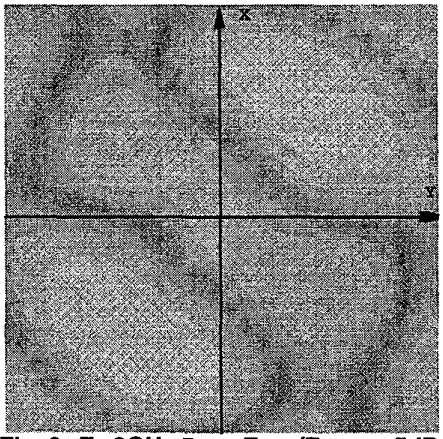

Fig. 8. E_y, 2GHz 5cm, $E_{max}/E_{min} \approx$ 5dB.

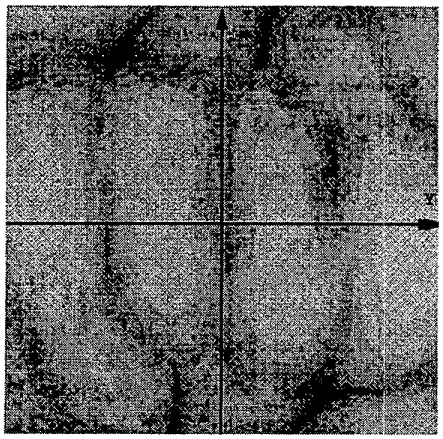

Fig. 9. E_z, 2GHz 5cm, $E_{max}/E_{min} \approx$ 16dB.

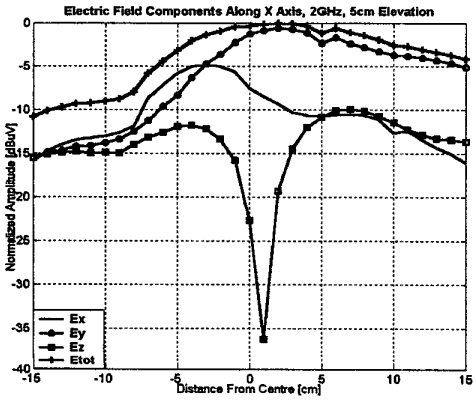

Fig. 10. Measured E at 2GHz/5cm, x-direction

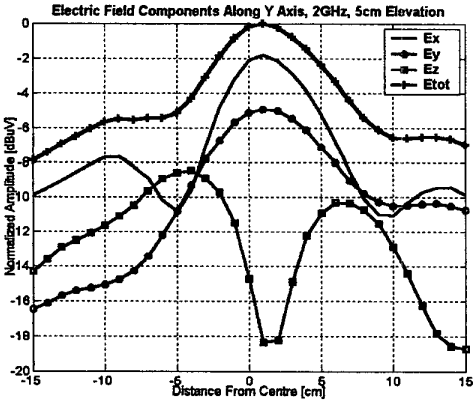

Fig. 11. Measured E at 2GHz/5cm, y-direction.

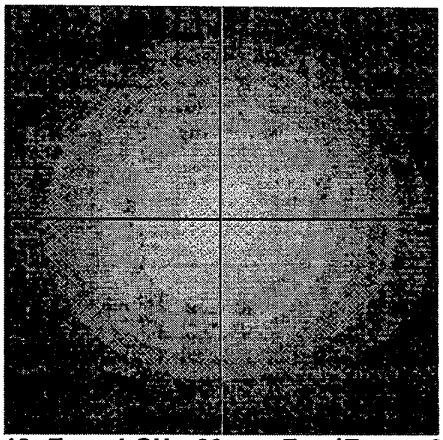

Fig. 12. E_{total}, 1 GHz, 20 cm, $E_{max}/E_{min} \approx$ 2 dB.

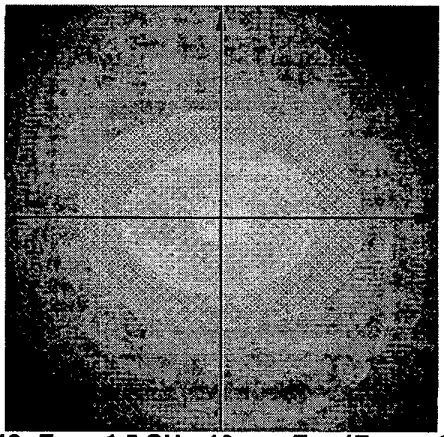

Fig. 13. E_{total}, 1.5 GHz, 10 cm, $E_{max}/E_{min} \approx$ 3 dB.

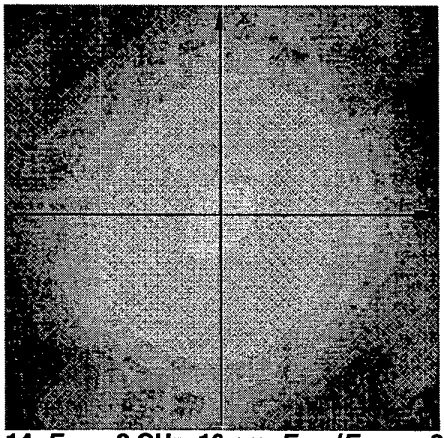

Fig. 14. E_{total}, 2 GHz, 10 cm, $E_{max}/E_{min} \approx$ 2 dB.

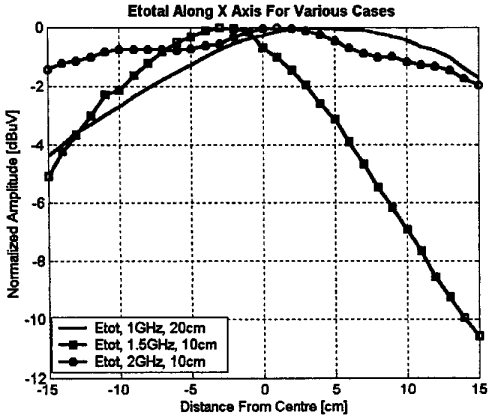

Fig. 15. Total E-field along *x*-direction.

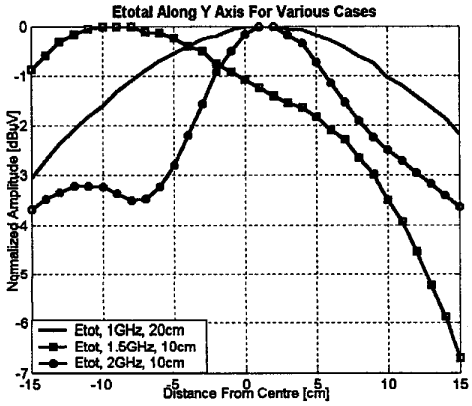

Fig. 16. Total E-field along *y*-direction.

Figures 12 through 14 show the simulated total electric field intensity E_{total} for z = 20 cm at 1 GHz, and for z = 10 cm at 1.5 GHz and 10 cm at 2 GHz, respectively. Figures 15 and 16 show the experimental data for these cases along the x and y axes. The experimental data show similar trends as in the simulations. The total electric field densities contain one main maximum centred at or near the antenna center (0 cm). One aberration for the case when the elevation plane is at 10 cm at 1.5 GHz along the y axis (Fig. 16.) where the field density maximum appears to be shifted by about 10 cm off center. Other minor unsymmetrical trends can be seen and are probably due to the balun.

5. Conclusions

Most of the experimental results are in agreement with the numerical simulations, confirming that the near field intensities can be very different from the far field patterns. However some peaks and valleys are not symmetrically distributed as expected in the numerical simulations. The most likely source of error for this experiment is a non-ideal balance delivered by the surface mounted ferrite balun. A cavity backed log-spiral antenna generally emits a single beam and displays no nulls in the far field over its operational bandwidth. This is not the case in the near field where multiple minima and maxima may occur. These characteristics may become important when a log-spiral antenna is used as a ground coupled GPR antenna where mines and mine-like targets will be located in close proximity to the antenna.

6. References

[1] J. Thaysen, K.B. Jakobsen, J. Appel-Hansen, "Characterisation and optimisation of a coplanar waveguide fed logarithmic spiral antenna," *2000 IEEE-APS Conference on Ant. and Prop. for Wireless Comm.*, pp. 25 -28, 2000

[2] R.V. de Jongh, A.G. Yarovoy, L. P. Ligthart, I.V. Kaploun, A.D. Schukin, "Design and analysis of new GPR antenna concepts," I*roc. GPR'98, 7th Int. Conf. on GPR*, Lawrence, Kansas, USA, Vol. I, pp. 81-86, May 27-30, 1998.

[3] B. Scheers, U*ltra-Wideband Ground Penetrating Radar, with Applications to the Detection of Anti-Personnel Landmines*, Ph.D. Thesis, Royal Military Academy, Dept. of Electrical Engineering, Brussels, March 2001.

[4] J.A.Cooke and M.T.Gladwin, "Ground Penetrating Radar Performance in Typical Australian Soils," www.cat.csiro.au/dem/msg/scirev/revradar.pdf

[5] G. Alberti, L. Ciofaniello, M. Della Noce, S. Esposito,G. Galiero, R. Persico, S. Vetrella, "Advanced stepped frequency GPR development," *Proc. of the Conf. on Subsurface Sensing Technologies and Applications II*, at SPIE's Annual Meeting, San Diego, USA., 2000.

[6] A.G. Yarovoy and L.P. Ligthart, "Ultra-wideband antennas for ground penetrating radar," *Proc. Int. Symp. on Ant. for Radar Earth Observation*, Delft University of Technology, The Netherlands, pp. 1-5, 8-9 June 2000.

[7] V. H. Rumsey, *Frequency Independent Antennas*, Academic Press, New York, 1966.

[8] M.N. Afsar, Y. Wang, H. Ding, "A new wideband cavity-backed spiral antenna," *Ant. and Prop. Soc. 2001 IEEE Int. Sym.*, vol. 4 , pp. 124 -127, 2001

[9] E. Gschwendtner, W. Wiesbeck, "Low-Cost Spiral Antenna with Dual-Mode Radiation Pattern for Integrated Radio Services," Institut für Höchstfrequenztechnik und Elektronik.

[10] J.L.Volakis, M.W. Nurnberger, D.S. Filipovic, "A Broadband Cavity-Backed Slot spiral Antenna," *IEEE Ant. and Prop. Magazine*, Vol. 43, No. 6, Dec. 2001, pp. 15 -26.

[11] C. A. Balanis, *Antenna Theory*, Second Edition, John Wiley & Sons, Inc., NY, 1997.